ARCHIVIO ISTITUZIONALE
DELLA RICERCA

Alma Mater Studiorum Università di Bologna
Archivio istituzionale della ricerca

Dual fluorescence through Kasha's rule breaking: An unconventional photomechanism for intracellular probe design

This is the final peer-reviewed author's accepted manuscript (postprint) of the following publication:

Published Version:
Brancato, G., Signore, G., Neyroz, P., Polli, D., Cerullo, G., Abbandonato, G., et al. (2015). Dual fluorescence through Kasha's rule breaking: An unconventional photomechanism for intracellular probe design. JOURNAL OF PHYSICAL CHEMISTRY. B, CONDENSED MATTER, MATERIALS, SURFACES, INTERFACES & BIOPHYSICAL, 119(20), 6144-6154 [10.1021/acs.jpcb.5b01119].

Availability:
This version is available at: https://hdl.handle.net/11585/530941 since: 2016-01-14

Published:

DOI: http://doi.org/10.1021/acs.jpcb.5b01119

Terms of use:

Some rights reserved. The terms and conditions for the reuse of this version of the manuscript are specified in the publishing policy. For all terms of use and more information see the publisher's website.

This item was downloaded from IRIS Università di Bologna (https://cris.unibo.it/).
When citing, please refer to the published version.

(Article begins on next page)

02 September 2024

This is the final peer-reviewed accepted manuscript of:

Brancato G, Signore G, Neyroz P, Polli D, Cerullo G, Abbandonato G, Nucara L, Barone V, Beltram F, Bizzarri R. Dual fluorescence through Kasha's rule breaking: an unconventional photomechanism for intracellular probe design. J Phys Chem B. 2015 May 21;119(20):6144-54. doi: 10.1021/acs.jpcb.5b01119. Epub 2015 May 12. PMID: 25902266.

The final published version is available online at: https://pubs.acs.org/doi/10.1021/acs.jpcb.5b01119

Rights / License:

The terms and conditions for the reuse of this version of the manuscript are specified in the publishing policy. For all terms of use and more information see the publisher's website.

This item was downloaded from IRIS Università di Bologna (https://cris.unibo.it/)

When citing, please refer to the published version.

Dual Fluorescence through Kasha's Rule Breaking: An Unconventional Photomechanism for Intracellular Probe Design

Giuseppe Brancato,*[,†] Giovanni Signore,[‡] Paolo Neyroz,[§] Dario Polli,[∥] Giulio Cerullo,[∥] Gerardo Abbandonato,[†] Luca Nucara,[‡] Vincenzo Barone,[†] Fabio Beltram,[‡,⊥] and Ranieri Bizzarri*[,⊥,#]

[†]Scuola Normale Superiore, Piazza dei Cavalieri 7, I-56126, Pisa, Italy

[‡]Center for Nanotechnology Innovation @ NEST, Istituto Italiano di Tecnologia, Pisa, Italy

[§]Dipartimento di Farmacia e Biotecnologie (FaBit), Università di Bologna, Via San Donato 19/2, 40127 Bologna, Italy

[∥]IFN-CNR, Dipartimento di Fisica, Politecnico di Milano, P. za L. da Vinci 32, 20133 Milano, Italy

[⊥]NEST, Scuola Normale Superiore and NANO−CNR, Pisa, Italy

[#]Istituto di Biofisica−CNR, via Moruzzi 1, 56124, Pisa, Italy

ABSTRACT: Dual fluorescence is an anomalous photophysical phenomenon observed in very few chromophores in which a two-color radiative process occurs that involves two distinct excited electronic states. To date its observation was linked either to electronic rearrangement of an excited fluorophore leading to two conformers with distinct emissive properties, or to a photochemical modification leading to different fluorescent species. In both cases, emission originates from the lowest excited state of the resulting molecular configurations, in line with the so-called Kasha's rule. We report here a combined theoretical and spectroscopic study showing, for the first time, an anti-Kasha dual-emission mechanism, in which simultaneous two-color emission takes place from the first and second excited state of a coumarin derivative. We argue that the observed environmental sensitivity of this peculiar optical response makes the present compound ideally suited for biosensing applications in living cells.

INTRODUCTION

In the last few decades, fluorescent chromophores drastically increased our capacity to monitor biological systems at the cellular and subcellular level. This prompted an intense effort toward the synthesis of new and ever more effective fluorescent probes sensitive to biologically relevant parameters.[1,2] Ideal probes should combine good emission properties in the visible (i.e., high quantum yield and long lifetime), high sensitivity toward specific cellular environments, and low (photo)toxicity. Another demanding and often required feature is the capability to provide a *quantitative* fluorescence signal irrespective of excitation-light intensity or probe concentration.[3] In this respect, one of the most appealing strategies involves the design of "self-calibrating" (ratiometric) fluorophores. These are probes that display a spectral modification upon interaction with a given biological target thereby providing a concentration-independent measurement through the ratio of fluorescence-intensity values measured at two selected wavelengths.[4,5] An interesting, but often overlooked, photophysical phenomenon to be exploited in the design of environmental-sensitive fluorophores is represented by *dual fluorescence*, i.e., an anomalous two-color radiative emission process involving two distinct excited electronic states of a fluorescent dye. Dual emission (DE) was originally reported in azulene derivatives at low temperature in 1974.[6] Later, it was observed in other chemical systems, such as carotenoids,[7] pyrylium salts,[8,9] naphthalimide,[10,11] and anthracene[12] derivatives, Zn−tetraphenylporphines,[13] and other fluorescent dyes.[14] In a few studies, the origin of DE was analyzed and linked to different mechanisms initiated by light. In some cases DE stems from a chemical modification of the dye leading to two different fluorescent species,[15] but more frequently, its origin was ascribed to the rearrangement of the fluorophore excited state following excitation. This was shown to lead to two distinct emissive conformations often associated with large electronic displacements.[16,17] In this latter case, DE can occur either sequentially, i.e., before and after the conformational rearrangement of the excited chromophore (as observed, for example, in 4,4′-dimethylaminobenzonitrile[18] (DMABN)), or concomitantly from two structurally different excited-state configurations.[14] To the best of our knowledge, in all reported cases DE was invariably attributed to the *lowest excited state* of the resulting molecular configurations according to the so-called *Kasha's rule*. This empirical rule is a milestone of spectroscopy which predicts that emission must occur from the lowest

This document is the Accepted Manuscript version of a Published Work that appeared in final form in . Phys. Chem. B 2015, 119, 6144-6154, copyright ©American Chemical Society after peer review and technical editing by the publisher. To access the final edited and published work see: http://dx.doi.org/10.1021%2Facs.jpcb.5b01119

excited state of a given multiplicity, irrespective of the initial photoexcited state.[19]

Here, we present a combined theoretical and spectroscopic study that shows, for the first time, a peculiar DE stemming from the simultaneous radiative decay from the first *and* second singlet excited state of a coumarin derivative, in the following referred to as **deC**. In contrast to all known dual emitters, the two excited states of **deC** are not formed or stabilized by any chemical or distinguishable structural change, thus showing a singular Kasha's rule breaking mechanism. Besides, the simultaneous generation of emitting states avoids the low quantum yield usually related to the first state of dual emitters characterized by a sequential excited-state rearrangement, arguably the true obstacle to their effective application in imaging studies. In our view, these photophysical features, along with a reported high sensitivity toward the environment in terms of both polarity and water content, make this fluorescent compound a promising tool for the implementation of new ratiometric indicators for functional cell imaging and a valuable template for the design of new molecular probes.[20]

MATERIALS AND METHODS

Solvents. All solvents were spectroscopic grade and were purchased from Sigma-Aldrich (Milan, Italy).

Chemical Synthesis. 3-(Benzo[*d*]thiazol-2-yl)-6,7-dimethoxy-2*H*-chromen-2-one-4-carbonitrile (**deC**), and its parent analogue 3-(benzo[*d*]thiazol-2-yl)-6,7-dimethoxy-2*H*-chromen-2-one (**seC**) were synthesized and purified according to the procedure reported in ref 20.

Samples for Spectroscopy. For steady-state and time-resolved fluorescence experiments, solutions of **deC** or **seC** in the selected solvents were placed in quartz cuvettes with 1 cm absorption/excitation optical path (Hellma, Milan, Italy); concentration of the fluorophore was adjusted to obtain 0.08−0.1 optical density and provide linearity between fluorescence emission and absorbance. For transient absorption experiments, solutions of **deC** in dichloromethane (DCM) were placed in quartz cuvettes with 0.1 cm absorption optical path; concentration of **deC** was adjusted to obtain 0.4−0.5 optical density, in order to provide optimal signal-to-noise ratio in the experiments.

Steady-State Optical Measurements. Absorption spectra were recorded at 25 °C by a JASCO V550 spectrophotometer (JASCO Europe, Italy) using 1 nm band-pass and 0.25 s integration time. Fluorescence intensity spectra were recorded at 25 °C by either a Cary Eclipse (Varian, Palo Alto, CA) or a Fluoromax-4 fluorometer (Jobin-Yvon, Milan, Italy) with 1−2 nm excitation/emission bandpass and 0.2−0.5 s integration time. Quantum yield and corrected fluorescence spectra were determined according to standard procedures.[21] For deconvolution, absorption or corrected emission spectra were fitted to a sum of Gaussian bands by IgorPro 6.2 (Wavemetrics, Lake Oswego, OR).

Time-Resolved Fluorescence Emission. Time-resolved fluorescence emission measurements were performed at 25 °C in a 90° geometrical excitation−emission configuration[22] by the time-correlated single-photon counting (TCSPC) approach, using a IBH 5000 (Jobin-Yvon) lifetime system equipped with a flash lamp (40 kHz at 50 kPa H_2). S_{10} transition was selectively targeted by exciting at 480 nm and collecting at 550 nm. The S_{20} transition was selectively targeted by exciting at 360 nm and collecting at 430 nm. In all cases emission was collected with 54.7° polarization (magic angle) with respect to excitation polarization. Data were collected into 1024 channels at a digital resolution of 0.103 ns per channel. Lifetime values were determined by fitting the emission decays with a multiexponential function convoluted with the experimental instrument response function (IRF) obtained by collecting the time-resolved scattering emission from a blank solution for each tested solvent. Decay curves collected at multiple emission wavelengths were analyzed simultaneously and used to resolve the decay-associated spectra (DAS).[23]

Dynamic Anisotropy. Following the same scheme as for time-resolved fluorescence, decays were collected in the parallel (I_{VV}) and perpendicular (I_{VH}) directions with respect to vertical excitation polarization by a Fluoromax-4 fluorometer (Jobin-Yvon) equipped with a FluoroHub-B TCSPC system and a NanoLed source (390 or 455 nm, 1 MHz). To retrieve time-resolved anisotropy, I_{VV} and I_{VH} were concomitantly analyzed by multiexponential functions convoluted with system IRF (fitting software: Fluofit, Picoquant, Berlin) after determination of the *G* factor by standard means.[22]

Transient Absorption. Experiments were carried out using a homemade ultrafast pump−probe setup[24] based on an amplified Ti:sapphire system (Quantronix model Integra-C) delivering fundamental pulses at 1-kHz repetition rate, 800 nm central wavelength and 100 fs duration. Pump pulses at 400 nm were generated by frequency doubling the fundamental wavelength in a β-barium borate crystal. Probe pulses spanning the 330−750 nm wavelength range were obtained by single-filament supercontinuum generation in a CaF_2 plate with 3 mm thickness, which was continuously translated in the plane perpendicular to the laser beam to avoid damage and color-center formation. Probe pulses were delayed with respect to the pump pulses using a computer-controlled linear translation stage (Physik Instrumente model M-521.2S, with 200 nm position repeatability, corresponding to ≈1.3 fs delay accuracy). Pump pulses were modulated using a mechanical chopper at 500-Hz frequency, synchronized with the laser repetition rate. Detection of each probe spectrum at the full 1-kHz rate was performed using a high-speed camera (Entwicklungsbuero Stresing) based on a 1024-pixel CCD sensor from Hamamatsu (model S7030−1006, with full vertical binning) mounted on a 30 cm focal-length imaging spectrometer (Princeton Instruments, Acton series).

Cell Cultures. U2OS cells were grown in Dulbecco's modified Eagle medium: F-12 nutrient mix (D-MEM/F-12) purchased from Invitrogen (Carlsbad,CA) supplemented with 10% fetal bovine serum and 100 U/ml penicillin, and 100 mg/mL streptomycin (Invitrogen). Cells were maintained at 37 °C in a humidified 5% CO_2 atmosphere. Cells were incubated for 24 h before imaging. For live imaging, cells were plated onto 35 mm glass bottom dish (WillCo-dish GWSt-3522) 24 h prior to experiments at 60−80% confluence. For the experiments the cells were loaded for 15−30 min with compounds **1** or **3** (0.5−1 μM). The fluorescent probe, solubilized in DMSO (1 mM), was dissolved directly in cell medium.

Confocal Imaging of Cells. Fluorescence imaging was done using a Leica TCS SP5 SMD confocal microscope (Leica Microsystems, Mannheim, Germany) interfaced with two diode lasers (Picoquant) for excitation at 403 and 470 nm. U2OS cells in glass bottom Petri dishes were exposed to 1 μM **deC** in cell medium (DMEM) at 37 °C and viewed with a 40 × 1.25 NA water immersion objective (Leica Microsystems, Berlin, Germany). The images were collected using low excitation power at the sample (10−20 μW) and monitoring the emission

by means of an Acousto Optical Beam Splitter (AOBS)-based built-in detectors of the confocal microscope. Data were analyzed by ImageJ software (National Institutes of Health, Bethesda, MD).

Computational Details. Quantum mechanical (QM) calculations of the structure and optical properties were carried out by methods rooted into density functional theory (DFT) and its time-dependent extension (TD-DFT).[25,26] As shown in previous studies, hybrid functionals (here PBE0[27,28] and B3LYP[29,30]) and their long-range corrected extensions (here, CAM-B3LYP)[31] are appropriate for describing optical properties of molecular systems, even with an extended electronic delocalization. The 6-31+G(2d,p) basis set was used in all calculations. Solvent effects were included implicitly by the conductor version of the polarizable continuum model (C-PCM).[32−34] Vertical transition energies were computed within the usual linear-response approximation for the case of optical absorption, whereas state-specific PCM calculations were performed for optical-emission calculations using fully relaxed excited-state geometries and the proper nonequilibrium regime.[35,36] Vibronic effects were accounted for by an effective time-independent approach, including Franck−Condon, Herzberg−Teller, and Duschinsky effects.[37] The stick spectra were first generated and then convoluted using Gaussian distribution functions with half-widths at half-maximum of 550 cm^{-1}. Since the complete adiabatic Hessian (AH) and the simplified vertical gradient (VG) approaches provide comparable results, interpretations were based on the simpler VG method.[38] All quantum mechanical calculations were carried out with the Gaussian09 software package.[39]

RESULTS AND DISCUSSION

Structural Properties. The fluorescent **deC** coumarin is characterized by a *push−pull* hyperconjugated molecular system (Scheme 1). Two methoxy groups in position 6 and 7 of the coumarin core work as "electron-donating" (*push*) units, whereas the benzothiazenyl and cyano groups, respectively in position 3 and 4, play the electron-withdrawing (*pull*) function. Quantum-mechanical calculations showed that the optimized ground-state structure of **deC** corresponds to a planar conformation with the methoxy groups coplanar with the coumarin core, whereas other low-energy minima displayed the methoxy groups arranged in different orientations (see Figure S1). At room temperature, the bulky benzothiazene group is considered stable in a coplanar configuration with the rest of the molecule, owing to a stabilization energy of about 4 kcal/mol. Moreover, in the first two excited states the rotational barrier of the benzothiazene group is increased as a result of the electronic density shift toward the C−C bond linking such a group to the coumarin scaffold (see discussion below).

Scheme 1. Chemical Structure of Dual-Emitting Benzothiazenyl Coumarine deC

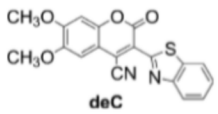

deC

Steady-State Optical Properties. The steady-state optical properties of **deC** were investigated in different solvents to test the effect of different environments. On account of the strong specific effect of solvent H-bonding on **deC** emission,[20] we purposely selected mild H-bonding or aprotic solvents, namely: ethyl acetate (EA), dichloromethane (DCM), poly(ethylene glycol) 400 (PEG400), 2-propanol (IP), and acetonitrile (ACN). Note that PEG400 is characterized by a dielectric constant ε = 17.3,[40] similar to IP (ε = 18.3), although its viscosity is about 46 fold higher (PEG400, η = 94.4 cP;[41] IP, η = 2.04 cP, 298 K)

In the visible range, **deC** displayed an intense and structured absorption band peaked near 460 nm, hereafter denoted by S_{01}, together with a significant shoulder at λ < 410 nm, hereafter denoted by S_{02}, (Figure 1a). Spectral deconvolution afforded the two S_{01} and S_{02} bands (Figure 1a, dotted lines), whose molar absorption coefficients (ε_1, ε_2) and peak wavelengths (λ_1, λ_2) are reported in Table 1. Note that although solvent polarity and H-bonding decreased somewhat ε_1 and ε_2, λ_1 and λ_2 evidenced instead only little dependence on solvent polarity.

Fluorescence spectra displayed a peculiar emission pattern depending on the excitation wavelength. Selective excitation of S_{01} (λ_{ex} > 480 nm) led to single fluorescence emission (SE) peaking at 560−580 nm (Figure 1b); the associated broad band will be hereafter denoted as S_{10}. Conversely, selective excitation of S_{02} (λ_{ex} = 300−380 nm) yielded anomalous dual-emission (DE) spectra: in addition to the previously observed S_{10}, a second weaker band appeared between 450 and 500 nm, hereafter denoted as S_{20} (Figure 1c). Deconvolution analysis of the fluorescence spectra provided further insight on the photophysical behavior of **deC**. S_{10} was resolved into four sub-bands, whose maxima (λ_{10a}, λ_{1b}, and λ_{1c}) were found to red-shift by ≈10−40 nm upon increasing solvent polarity (Table 2). Conversely, S_{20} was resolved into two sub-bands notably insensitive to solvent polarity. The DE regime was fully quenched in water on account of specific solute−solvent hydrogen-bonding interactions:[20] only S_{20} remained active, albeit with very dim fluorescence (see Figure S2).

Spectroscopic Calculations. QM calculations of excitation energies showed that at most three electronic transitions from the ground state fall into the optical absorption range considered in the steady-state experiments ($\lambda_{ex} \geq$ 350 nm). Each of these transitions is described to a good approximation by a one-electron excitation from the HOMO, $HOMO^{-1}$, or $HOMO^{-2}$ orbitals to the LUMO orbital (a relative weight of the main excitation of about 0.70 was obtained in each case), as depicted in Figure 2a. Note that the LUMO is characterized by a partial electronic localization onto the cyano moiety in contrast with the other frontier orbitals. In particular, the HOMO and $HOMO^{-2}$ are essentially delocalized onto the coumarin aromatic scaffold while the $HOMO^{-1}$ is mostly localized onto the benzothiazene group (Figure 2a). As a result, depending on the relative orientation of the methoxy groups, the absorption energies in ACN corresponding to S_{01} and S_{02} were estimated to lie in the range λ_{abs} = 440−500 nm and λ_{abs} = 380−415 nm, respectively, in excellent agreement with experiments (Table 1). In terms of electronic rearrangement, we observed a relative shift of the electron density from either the coumarin aromatic rings (S_{01}) or the benzothiazene group (S_{02}) toward the cyano functional group (see Figure S3). In the first excited states, the CN bond undergoes an elongation by about 0.01 Å, while the neighboring CC bond is shortened by about 0.03 Å. A similar decrease of about 0.03 Å also affects the CC bond connecting the benzothiazene group to the rest of the molecule (from about 1.46 Å in the ground state to 1.42−1.43 Å in the excited states), as if it acquires a partial double-bond character that, in turn, makes stiffer the torsional potential

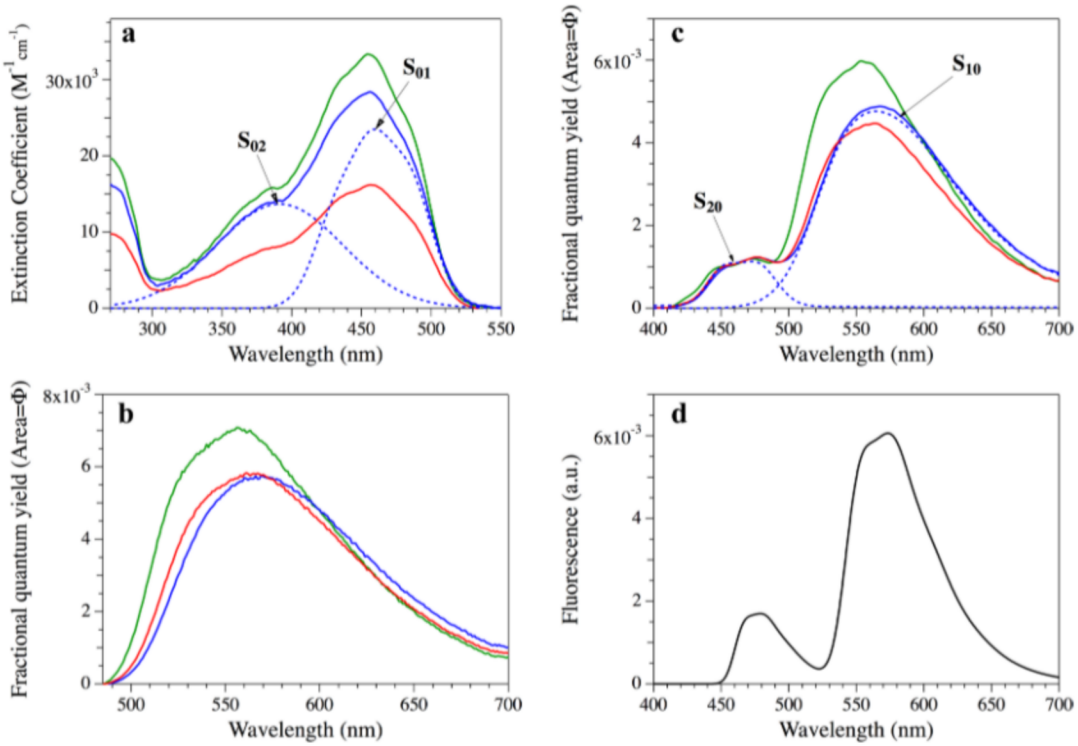

Figure 1. (a) Absorption spectra of **deC** in EA (dark green), ACN (blue), and IP (red): transitions S_{01} and S_{02} in ACN are displayed as blue dashed lines. (b) Corrected emission spectra upon excitation at 480 nm with same color code as in part a. (c) Corrected emission spectra upon excitation at 360 nm with same color code as in part a; transitions S_{10} and S_{20} in ACN are displayed as blue dashed lines. (d) Emission spectrum of **deC** from QM calculations. Note that, in parts b and c, each emission spectrum is intensity-normalized as such as its area amounts to the quantum yield of **deC** in the solvent where it is measured; thus, in these plots, the units of the *y*-axis are absolute numbers.

Table 1. Optical Absorption Properties of deC

		S_{01}		S_{02}	
solvent	ε	λ_{01} (nm)	ε_{01} (M^{-1} cm^{-1})	λ_{02} (nm)	ε_{02} (M^{-1} cm^{-1})
EA	6.0	458	30 100	386	12 200
DCM	9.1	463	29 800	396	12 500
PEG400	17.3	467	21 500	390	7100
IP	18.3	459	27 000	391	12 400
ACN	37.6	460	23 500	392	13 700

energy of such a substituent group. Overall, the excited-state geometries showed strong similarities with the ground-state geometry. In addition, the **deC** dipole moment has slightly changed in going from the ground state to the excited states (μ_{S0} = 6.1 D; μ_{S1} = 8.2 D; μ_{S2} = 5.0 D), considering relaxed geometries upon excitation. It is worth noting that such small electronic and structural rearrangements are consistent with the observed asymmetric band shapes in both optical absorption and emission spectra, as due to the Franck−Condon progression.

Our QM investigation showed that the peculiar dual-fluorescence response is not due to vibronic effects modulating a single emissive process, but rather to two distinct and simultaneous de-excitation processes, as issuing from S_1 and S_2 states. Solvent effects, as well as Franck−Condon factors, do affect each electronic transition and modulate the corresponding band shape but do not account for the observed DE. Figure 1d reports an example of vibronic fluorescence spectra calculated within the vertical gradient approximation and displays a good agreement with the recorded spectra.

The prevalent localization of the LUMO onto the cyano group, as well as its role on both excitations, motivated a further investigation on the role of this substituent. Interestingly, while the spatial localization of the HOMO and HOMO^{-1} molecular orbitals was found to be very similar in a **deC** analogue lacking the cyano group (**seC**), the LUMO was observed to strongly differ from the parent compound (Figure 2b). The steady-state optical spectra of **seC** display two absorption bands, similarly to **deC**, but no DE feature in emission (both spectra are blue-shifted by 70−100 nm as compared to **deC**, Figure 3). These

Table 2. Fluorescence Emission and Lifetime Properties of deC

	S_{20}				S_{10}					
solvent	λ_{20a} (nm)	λ_{20b} (nm)	Φ_{S2}	τ_2 (ns)	λ_{10a} (nm)	λ_{10b} (nm)	λ_{10c} (nm)	λ_{10d} (nm)	Φ_{S1}	τ_1 (ns)
EA	446	471	0.18	2.93	518	545	578	626	0.96	5.54
DCM	450	474	nd	nd	524	553	589	640	0.83	5.37
PEG400	455	480	nd	3.01	535	562	597	649	0.59	4.42
IP	449	475	0.19	2.75	531	556	589	640	0.77	4.74
ACN	449	474	0.36	3.27	526	553	591	670	0.76	5.28

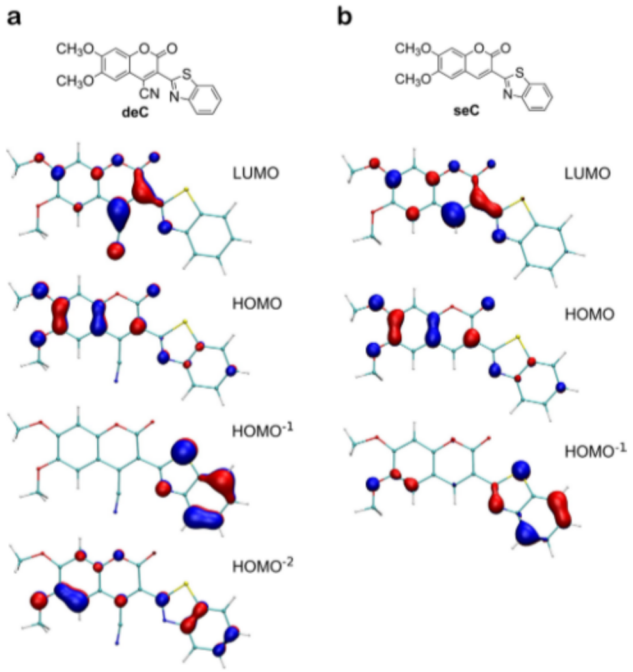

Figure 2. Graphical representations of the highest occupied (HOMOs) and lowest unoccupied (LUMO) molecular orbitals of **deC** (A) and **seC** (B). Note that the first electronic transitions from the ground state fairly correspond to one-electron excitations from the HOMO, $HOMO^{-1}$ and $HOMO^{-2}$ orbitals, respectively, to the LUMO orbital (in each case, a relative weight of about 0.70 was obtained). At variance with **deC**, the LUMO of **seC** is mostly localized onto the coumarin scaffold due to the lack of the cyano moiety. On the other hand, the spatial localizations of the HOMO and $HOMO^{-1}$ molecular orbitals of **seC** resemble the ones observed in **deC**.

findings support the pivotal role played by the cyano moiety in triggering the observed DE.

Time-Resolved DE Properties: the ns Time Scale. The >200 ps lifetime of **deC** was measured by pulse fluorometry[22]

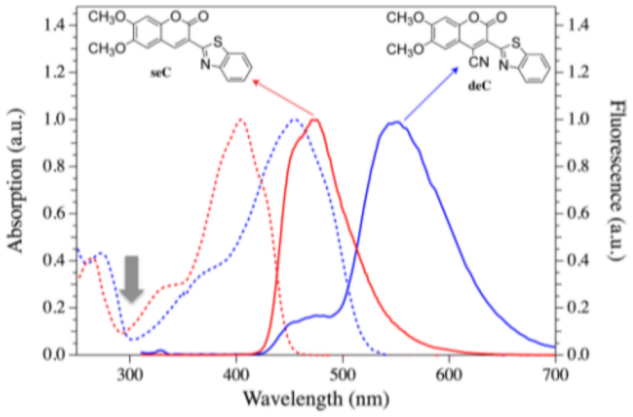

Figure 3. Absence of CN group in **seC** as compared to the parent analogue (**deC**) hampers the dual fluorescence emission. The plot shows the absorption and emission spectra of **seC** and **deC** in ACN, for comparison (the corresponding chemical structures are also reported). In both cases, the absorption spectra show visible overlap of two bands. Yet, excitation at 300 nm (i.e., the high energy band, see gray arrow) yields DE from **deC**, while **seC** shows a typical single fluorescence band.

at variable excitation and emission wavelengths (resolution: 140 ps). Excitation at 480 nm and collection at 550 nm (Figure 4a)

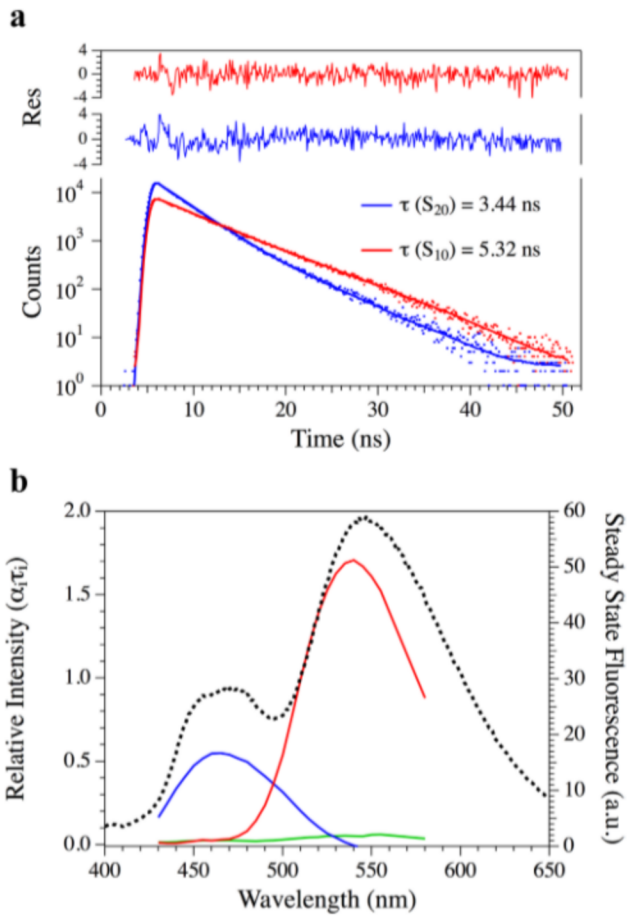

Figure 4. (a) Time-resolved emission decay of **deC** in ACN relevant to transitions S_{10} (red trace) and S_{20} (blue trace). S_{10} decay was obtained by excitation at 480 nm and collection at 550 nm; S_{20} decay was obtained by excitation at 350 nm and emission at 460 nm. In both cases traces were fitted to a monoexponential function to recover the lifetime; full lines represent fits and residuals are shown in the upper part of the plot. (b) Left scale: DAS relevant to emission decays collected from 430 to 580 nm upon excitation at 360 nm (S_{02}): colors refer to the three lifetime components of the global fitting: τ_1 (red), τ_2 (blue), τ_3 (green). Right scale: the steady-state emission spectrum at the same excitation wavelength is reported as dashed black curve for reference.

selectively afforded the decay pattern of S_{10} in the SE regime. S_{10} was associated with a monoexponential decay with lifetime τ_1 ranging from 4.42 ns in PEG400 to 5.54 ns in EA (Table 2), in agreement with previously reported data.[20] The DE regime was investigated by exciting at 360 nm and collecting from 430 to 580 nm in order to obtain the decay associated spectra[42] (DAS, Figure 4b). For DAS, the fluorescence decays were fitted globally by assuming three distinguishable lifetime components whose one represented by previously determined τ_1. Comparison with steady-state spectra indicated that DAS components 1 and 2 correlate well with the steady-state S_{10} and S_{20} emissions (Figure 4b). The blue shift of S_{10} in DAS as compared to the steady-state spectrum has an instrumental origin (it can be attributed to the different detection efficiency at $\lambda > 500$ nm of the lifetime TCSPC fluorometer with respect to the steady-

state fluorometer). At wavelengths where only S_{10} is emitting (>550 nm), the amplitude of the lifetime component relevant to S_{20} emission was found to be negligible compared to that of S_{10}. This means that S_{20} and S_{10} transitions are not related by a *precursor–successor* relationship. Indeed, in such a case, one would expect similar amplitudes with opposite sign when S_{10} only is emitting, owing to the depopulation of S_2 in favor of S_1.[43] The third DAS component was associated with a very fast decay and a negligible intensity throughout the wavelength range. This band was attributed to a minor drift of the instrument response function during the experiments.

Time-Resolved DE Properties: the fs–ps Time Scale. The photophysical behavior of **deC** at >200 fs following photoexcitation was investigated by means of femtosecond transient absorption measurements. The pump–probe system operated at the pump wavelength of 400 nm, thus exciting mainly S_{02}, while probing the 430–660 nm interval. DCM was selected as solvent on account of the high solubility of **deC** in this medium; an optical density as high as 0.4–0.5 in the 1 mm optical path of our quartz cell was used. Figure 5a shows the ΔA spectra from −600 to +1600 fs delay. Two *negative* bands peaking at 470–475 (N_2) and 560–570 nm (N_1), and one *positive* band peaking at 520–525 (P_1) are clearly observable.

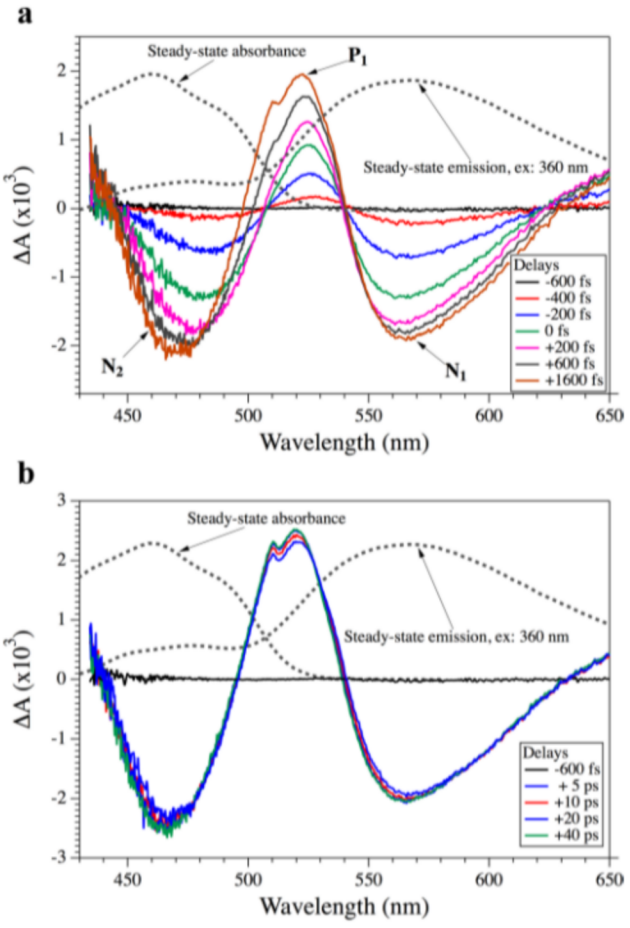

Figure 5. Transient absorption spectra of **deC** upon excitation at 390 nm. The vertical axis represents the differential absorbance (ΔA) of solution. Two windows of delay times between pump and probe are reported: (a) −600 to 1600 fs, and (b) −600 fs to 40 ps. For comparison, in both panels the steady-state absorbance and fluorescence (exc: 360 nm) of **deC** are reported as dotted black lines.

Comparison with steady-state absorption and emission spectra (Figure 5a,b, dashed lines) indicates that N_2 can be assigned to the superposition of ground-state bleaching and stimulated S_{20} emission. N_1 can instead be ascribed only to stimulated S_{10} emission due to the lack of ground-state absorption and of fluorescence from S_2 in this spectral range. Finally P_1 can be assigned to photoinduced absorption from either S_1 or S_2 to a higher-lying excited state. Yet, the presence of a stationary isosbestic point at 540 nm between P_1 and N_1 indicates a common origin, thus suggesting that P_1 absorption takes place from S_1. Conversely, the isosbestic point between N_1 and P_1 blue-shifts from 507 to 480 nm within the first 800–1000 fs: given the constancy of the isosbestic point between P_1 and N_1, we attribute this mainly to a blue-shift of N_2 in the same time range.

The analysis of the time evolution of the transient absorption signals provides further information on the dual-emission process, as it shows that S_2 and S_1 are populated simultaneously or at least within the duration of the instrumental response function (IRF) of our system, which is ≈200 fs fwhm. Kinetics at 472, 522, and 565 nm probe wavelength (i.e., at the peak of N_2, P_1 and N_1 bands, respectively) are reported in Figure S4 together with a multiexponential fit. We employed a simple sequential three-state model consisting of: (i) a first Franck–Condon excited state ("hot" S_1 and S_2 states), which decays with rate constant k_1 into (ii) a subsequent relaxed form of S_1 and S_2, which in turn decays with rate constant k_2 back to (iii) the ground state. The numerical solution of the rate equations was then convoluted with a Gaussian function with fwhm duration equal to our IRF in order to take into account the finite temporal resolution of the measurements. The results of this fitting procedure show that 85% of N_2, 65.5% of P_1, and 87.5% of N_1 are populated within the IRF and are to be considered "instantaneous" for our measurements (see the yellow shaded area in Figure S4). Subsequently, signals rise at all probe wavelengths on the picosecond time scale, as evident both from the spectra at various delays in Figures 5 and the kinetic traces in Figure S4. The fits allow us to extract the time constants $\tau_1 = (k_1)^{-1}$ associated with these *formation* processes: 4.38 ps (N_2), 2.2 ps (P_1), and 8.7 ps (N_1). Decay of these signals back to the ground state occur on the nanosecond time scale, as evident from the plateau reached at 50 ps delay in Figure S4 (time constant $\tau_2 = (k_2)^{-1} \gg 50$ ps). On the basis of these observations, we can conclude that S_1 and S_2 are concomitantly populated within the first hundred femtoseconds upon excitation to the Franck–Condon state, and no later evolution of S_2 into S_1 occurs. The slower processes (τ_1 = 2–8 ps) may be related to some minor structural rearrangement of the excited states. Solvent dipolar relaxation must be excluded, since the average dipolar relaxation time of DCM around excited Coumarin 153 is about 560 fs.[44]

Time-Resolved Anisotropy Measurements. The depolarization dynamics of **deC** was investigated by pulse fluorometry[22] in order to determine the fundamental anisotropy r_0 (i.e., the anisotropy index in absence of any rotational motion) attributable to S_{20} and S_{10} upon excitation of the S_{02} transition. Note that, with good approximation, assuming that other depolarization effects are negligible, r_0 is directly linked to the α angle between excitation and emission transition dipole moments through the formula:[22]

$$r_0 = 0.4\frac{3\cos^2\alpha - 1}{2} \quad (1)$$

Small dyes such as coumarines display rotational correlation time (θ) in the 10−100 ps interval in nonviscous organic solvents, and detection of emission depolarization requires high-temporal-resolution spectroscopy.[45] To avoid this, time-resolved anisotropy was monitored in viscous PEG400, thus slowing down the rotational times to the nanosecond range. We generated the dual fluorescence by exciting the chromophore at 390 nm and collected the time-dependent emission both at 460 nm (monitoring S_{20}) and 560 (probing S_{10}). Emission decays parallel and perpendicular to the excitation were fitted by a single-rotor model assuming equal θ for both emission wavelengths. We found $\theta = 6.1$ ns, $r_0(S_{20}) = 0.38 \pm 0.01$, and $r_0(S_{10}) = 0.290 \pm 0.005$. From these data, we calculated $\theta = 30.5$ ps in DCM, in excellent agreement with the typical correlation rotational times found for coumarine analogues.[45] By means of eq 1, the measured r_0 values were converted into the α angles between excitation and emission transition dipole moments[22] obtaining $\alpha(S_{20}) = 10.2°$ and $\alpha(S_{10}) = 25.1°$. Under the assumption of coplanar emission transition moments, $\Delta\alpha = \pm 14.9°$. Remarkably, QM calculations of **deC** in ACN indicated the two emission transition moments be truly coplanar with $\Delta\alpha = 15°$, as obtained by considering different **deC** conformations. This agreement further substantiates the theoretical characterization of excited states and the related DE properties.

Features of DE Mechanism. All the presented experimental and theoretical findings converge to show that an anomalous photophysical mechanism based on a Kasha's rule violation is at the basis of the observed DE response of **deC**. To summarize: (a) two electronic transition bands are clearly distinguishable in both absorption and emission spectra; (b) excitation of the low-energy absorption band (S_{01}) leads to single emission, whereas excitation of the high-energy absorption band (S_{02}) leads to DE; (c) the computed molecular dipole moment and geometry are only slightly affected by solvent and electronic excitation; (d) lifetimes and fundamental anisotropies of S_{10} and S_{20} are different; (e) the Franck−Condon excited state evolves to S_{10} and S_{20} within 200 fs after excitation.

The present anti-Kasha DE mechanism is illustrated by a simple Jablonski diagram (Scheme 2). First, excitation of S_{02} leads to a nonrelaxed Franck−Condon S_2 state (FC-S_2). Next, FC-S_2 undergoes internal conversion to S_1 in less than 200 fs with probability (quantum efficiency) η: at such an early time the initial excited-state population is split and decoupled along S_1 and S_2 ever since. Therefrom, relaxation along the vibrational sublevels of S_2 and S_1 occurs in ps, and eventually fluorescence emission occurs in ns.

Scheme 2. Jablonski Diagram Describing the Anti-Kasha DE of deC[a]

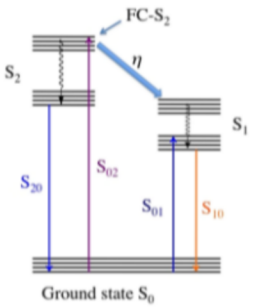

[a]Activation of the S_{02} transition leads to a Franck−Condon nonrelaxed state (FC-S_2) that, within a few tens of femtoseconds, undergoes an internal conversion to S_1 with quantum efficiency η. Then, thermal relaxation along the vibrational sublevels of S_2 and S_1, followed by emission from both states, do occur in a fully decoupled way.

The quantitative features of the FC-S_2 → S_1 internal conversion were investigated in EA, IP, and ACN by evaluating both the emission intensity ratio between S_{10} and S_{20} (Φ_{dS1}/Φ_{dS2}) and η for excitation from 300 nm up to 425 nm (see theoretical description in Appendix 1). In all solvents, Φ_{dS1}/Φ_{dS2} and η showed excitation-wavelength dependence with a distinguishable local maximum at $\lambda_{ex} = 350$ nm (Figure 6). In particular, η is significant ($\geq$0.6) in the whole range of λ_{ex} considered, with only a minor dependence on solvent polarity. Also, η decreases at longer excitation wavelengths consistently with a process that takes place from an upper vibrational level of S_2.

deC as Novel Dual Ratiometric Indicator of Environmental Polarity in Living Cells. We finally show how the peculiar photophysics of **deC** makes it operate on a novel paradigm that can yield *ratiometric dual-probe* functionality in living cells.

Solvatochromism of S_{10} emission is associated with a strong linear dependence of the generalized polarization (GP) parameter[46] on the logarithm of the local dielectric constant ε, similarly to another recently reported probes,[47] according to the following expression:

$$GP[\Delta\lambda_1, \Delta\lambda_2] = \frac{F_{\Delta\lambda_1} - GF_{\Delta\lambda_2}}{F_{\Delta\lambda_1} + GF_{\Delta\lambda_2}} = A + B\ln(\varepsilon) \quad (2)$$

In eq 2, $F_{\Delta\lambda 1}$ and $F_{\Delta\lambda 2}$ are the fluorescence intensities collected at two distinct wavelength ranges ($\Delta\lambda_1$ = 485−540,$\Delta\lambda_2$ = 545−635, Figure 7a) and G is a parameter that casts the different collection efficiency in the two intervals.[46] Notably, the linear *GP vs* $\ln(\varepsilon)$ relationship was found to hold, with similar slope, for both direct (λ >450 nm) and indirect (S_2→ S_1 conversion, λ <410 nm) excitation to S_1.

The stable efficiency of DE in various solvents (Figure 6) prompted us to analyze the dependence of (Φ_{dS1}/Φ_{dS2}) on polarity by recasting it in terms of *GP* (Figure 7b,c). Remarkably, we found out that *GP* [(425−480),(485−635)] is little influenced by polarity in organic solvents; conversely, it shows a nonlinear monotonic dependence on the volume fraction of water (φ) in water/organic solvent mixture that follows the relation:

$$GP = [(425 - 480), (485 - 635)] = C\exp(k\varphi) + D \quad (3)$$

where C, k, and D are empirical parameters. Note that, for $\varphi \rightarrow 1$, GP [(425−480),(485−635)] is close to zero (Figure 7c). Indeed, as already stated, at very high water content the DE regime is nearly abolished but about half of the S_{20} fluorescence is still collected in the 485−635 range (see Figure S2).

Equations 2 and 3 yield the simultaneous determination of ε and φ from *GP* [(485−540),(545−635)] and *GP* [(425−480),(485−635)], respectively, once a preliminary calibration of the empirical parameters is provided. As a first application, we set out to measure both these properties in **deC**-loaded living human osteosarcoma cells (U2OS) by confocal microscopy (Figure 8). We found out that **deC** senses $\langle\varepsilon\rangle = 9.3 \pm 3.6$ (#80 cells, Figure 8c), coherently with its predominant partition into

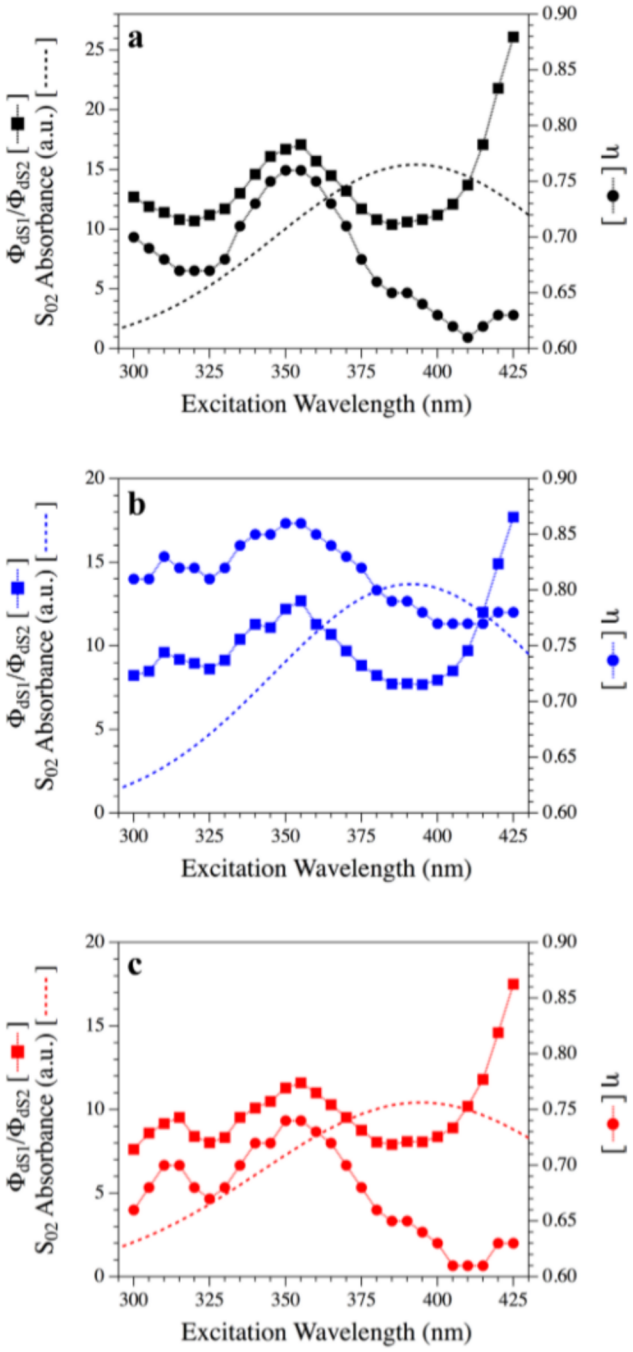

Figure 6. Dual emission steady state properties. Φ_{dS1}/Φ_{dS2} (squares), dual emission quantum efficiency η (circles), and S_{20} absorption (dotted line) vs excitation wavelength. Data refer to EA (panel a, black traces), ACN (panel a, blue traces), and IP (panel c, red traces).

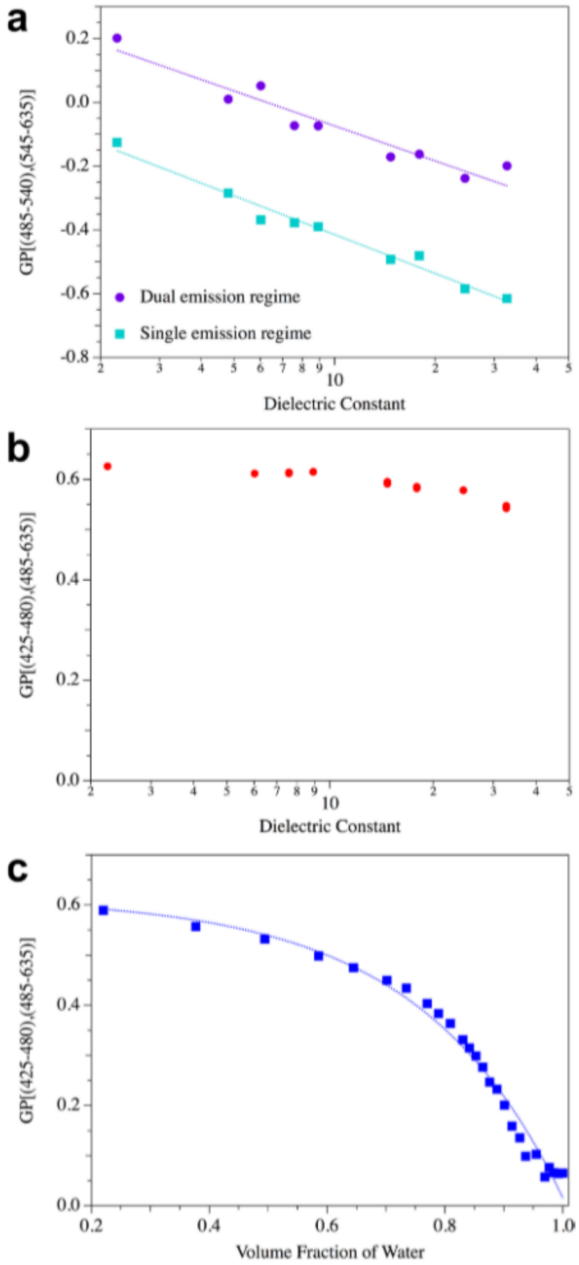

Figure 7. Generalized polarization (GP) of **deC** as a function of environmental polarity. (a) The S_{10} emission band is split into two wavelength intervals, 485−540 and 545−635 nm, and the relevant GP *vs* the logarithm of dielectric constant ε (see eq 2 in the text) is plotted for several solvents. Cyan points refer to single emission regime, as S_1 is directly reached by excitation at 458 nm; violet points refer to double emission regime, as S_1 is indirectly populated by excitation at 375 nm. In both cases, excellent linear trends of GP *vs* $\ln(\varepsilon)$ are obtained, as witnessed by the dotted lines. Note the similar slopes of GP *vs* $\ln(\varepsilon)$ obtained in the two cases, which supports the notion of same S_1 excited state responsible for the emission. (b, c) Under the dual emission regime (λ_{ex} = 375 nm), the Φ_{dS1}/Φ_{dS2} ratio is recast into *GP* and plotted vs either $\ln(\varepsilon)$ for a series of organic solvents (b) or the water volume fraction *j* for an 2-propanol/water mixture (c). Note that in both graphics have the same *y*-axis range to allow for quick comparison of the GP trends. In organic solvents, GP shows only a negligible dependence on polarity; conversely, minor amounts of water lead to significant changes of GP, likely on account of a specific H-bonding effect.

the membrane of lipophilic organelles such as the endoplasmic reticulum. A very similar $\langle\varepsilon\rangle$ value was recently measured by another solvatochromic fluorophore sensitive to local dielectric properties.[47] Besides, **deC** is partially entrapped in subcellular regions where >50% water in volume is present (Figure 8d). The clear overlap between ε and φ maps suggests that water-enriched regions are concomitantly imaged with the lipophilic ones at spatial scales below the resolution of the confocal microscope (200 nm on the image plane, 600 nm along the focal axis). We should note, however, that the copresence of

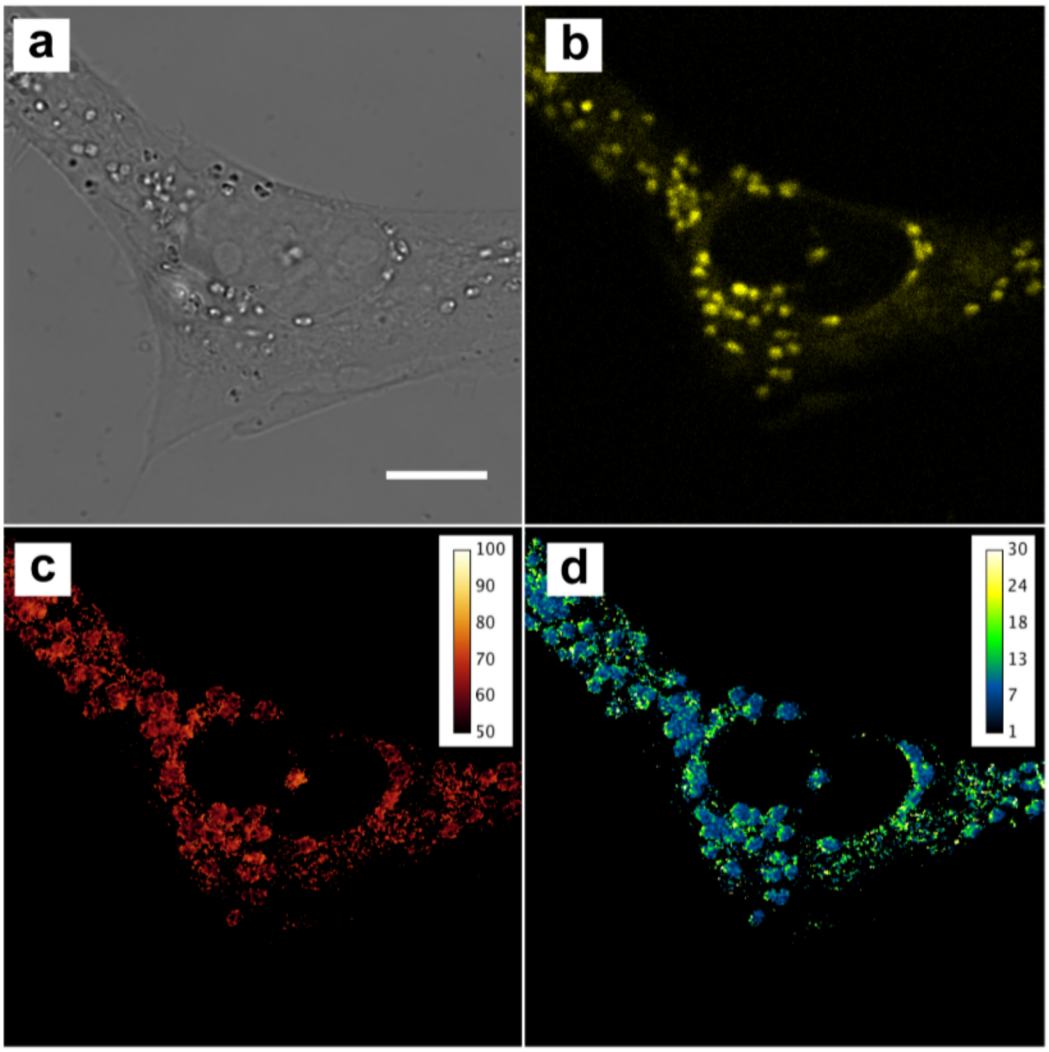

Figure 8. Confocal microscopy images of **deC** in U2OS cells. **deC**-loaded living U2OS cells were imaged by a confocal fluorescence microscope; fluorescence was collected in three different wavelength intervals: 425−480 nm (reporting mostly S_{20} emission), 485−540 nm (the "hydrophobic" range of S_{10} emission), and 545−635 nm (the "hydrophilic" range of S_{10} emission). Panels a and b show, respectively, the Normaski (transmission) and fluorescence intensity image (λ_{ex} = 470 nm, λ_{em} = 485−540 nm) of one U2OS cell. Scale bar: 10 mm. Panel c displays, by a thermal pseudocolor scale, the cellular map of water volume fraction (lower threshold 50%) as obtained from GP[(425−480),(485−635)] by applying eq 3 in the text. Panel d shows, by a 4-color scale, the cellular map of dielectric constant as obtained from GP[(485−540),(545−635)] by applying eq 2 in the text.

deC in both hydrophilic and hydrophobic locations is mainly due to its untargeted molecular form. The bioconjugation of **deC** to moieties such as lipids or proteins may target the probe to specific hydrophilic or hydrophobic regions of the cells where both dielectric constant and water content are consistent.

CONCLUSIONS

In conclusion, we investigated the peculiar dual fluorescence optical response of the **deC** coumarine. In contrast to all previously reported dual emitters at room temperature, here DE stems from a genuine Kasha's rule breaking mechanism thereby showing high efficiency and stability in different media. Such an anti-Kasha dual-fluorescence is, in our opinion, originated by the peculiar coexistence of three major factors in **deC**: (1) negligible structural rearrangement upon electronic excitation and subsequent relaxation, (2) optimal energy gaps of the two optical bands S_{02} and S_{01}, (3) fast (200 fs) internal conversion (Franck−Condon $S_2 \rightarrow S_1$) leading to a decoupled relaxation and simultaneous radiative decay from both S_2 and S_1. On account of its unique photophysics, **deC** was applied to cell imaging to report both polarity and water content of subcellular regions. This application may further benefit by the chemical functionalization of **deC** by engineering its phenyl-bound electron-rich groups in order to provide active sites for bioconjugation to moieties such as proteins. Notably, an effective functionalization synthetic approach has been already reported for the noncyan substituted **seC** analogue.[20,48]

In conclusion, we believe that our understanding of this peculiar DE may serve the purpose of developing a rational approach to the synthesis of a new generation of optical probes aiming at cell imaging applications.

ASSOCIATED CONTENT

Supporting Information

Calculation of internal conversion efficiency and Figures S1−S4, showing optimized geometries of deC, inhibition of S_{10} emission in water, graphical representations of the electronic density difference, and ps-scale absorption kinetics of deC. The

Supporting Information is available free of charge on the ACS Publications website at DOI: 10.1021/acs.jpcb.5b01119.

AUTHOR INFORMATION

Corresponding Authors

*(G.B.) Telephone: +39 050 509071. E-mail: Giuseppe.Brancato@sns.it.
*(R.B.) Telephone: +39 050 509522. E-mail: ranieri.bizzarri@nano.cnr.it.

Notes

The authors declare no competing financial interests.

ACKNOWLEDGMENTS

This work was partially supported by the European Union under the framework of the ERC Advanced Grant 2012 (Number 320951) and 2011 (Number 291198), and by the Italian Ministry for University and Research (MiUR) under the framework of FIRB Projects RBFR10DAK6 and RBPR05JH2P and PRIN Project 2010BJ23MN_004

REFERENCES

(1) Goncalves, M. S. Fluorescent Labeling of Biomolecules with Organic Probes. *Chem. Rev.* **2009**, *109*, 190−212.
(2) Chan, J.; Dodani, S. C.; Chang, C. J. Reaction-Based Small-Molecule Fluorescent Probes for Chemoselective Bioimaging. *Nat. Chem.* **2012**, *4*, 973−984.
(3) Kobayashi, H.; Ogawa, M.; Alford, R.; Choyke, P. L.; Urano, Y. New Strategies for Fluorescent Probe Design in Medical Diagnostic Imaging. *Chem. Rev.* **2010**, *110*, 2620−40.
(4) Demchenko, A. P. The Problem of Self-Calibration of Fluorescence Signal in Microscale Sensor Systems. *Lab Chip* **2005**, *5*, 1210−23.
(5) Demchenko, A. P. The Concept of Lambda-Ratiometry in Fluorescence Sensing and Imaging. *J. Fluoresc.* **2010**, *20*, 1099−128.
(6) Eber, G.; Grüneis, F.; Schneider, S.; Dörr, F. Dual Fluorescence Emission of Azulene Derivatives in Solution. *Chem. Phys. Lett.* **1974**, *29*, 397−404.
(7) Bettermann, H.; Bienioschek, M.; Ippendorf, H.; Martin, H.-D. Dual Fluorescence of Novel Modified Carotenoids. *Angew. Chem., Int. Ed.* **1992**, *31*, 1042−1044.
(8) Nikolov, P.; Metzov, S. Peculiarities in the Photophysical Properties of Some 6-Styryl-2,4-Disubstituted Pyrylium Salts. *J. Photochem. Photobiol., A* **2000**, *135*, 13−25.
(9) Pigliucci, A.; Nikolov, P.; Rehaman, A.; Gagliardi, L.; Cramer, C. J.; Vauthey, E. Early Excited State Dynamics of 6-Styryl-Substituted Pyrylium Salts Exhibiting Dual Fluorescence. *J. Phys. Chem. A* **2006**, *110*, 9988−94.
(10) Nandhikonda, P.; Heagy, M. D. Dual Fluorescent *N*-Aryl-2,3-Naphthalimides: Applications in Ratiometric DNA Detection and White Organic Light-Emitting Devices. *Org. Lett.* **2010**, *12*, 4796−4799.
(11) Nath, J. K.; Baruah, J. B. Solvatoemissive Dual Fluorescence of *N*-(Pyridylmethyl)-3-Nitro-1,8-Naphthalimides. *J. Fluoresc.* **2014**, *24*, 649−655.
(12) Muralidharan, S.; Yates, K. Bichromophoric Anthracene Derivatives with Dual Absorptive and Emissive States. *Chem. Phys. Lett.* **1992**, *192*, 571−575.
(13) Gurzadyan, G. G.; Tran-Thi, T. H.; Gustavsson, T. Time-Resolved Fluorescence Spectroscopy of High-Lying Electronic States of Zn-Tetraphenylporphyrin. *J. Chem. Phys.* **1998**, *108*, 385−388.
(14) Shen, D. W.; Bai, M. F.; Tang, R.; Xu, B. G.; Ju, X. M.; Pestell, R. G.; Achilefu, S. Dual Fluorescent Molecular Substrates Selectively Report the Activation, Sustainability and Reversibility of Cellular Pkb/Akt Activity. *Sci. Rep.* **2013**, *3*.
(15) Klymchenko, A. S.; Demchenko, A. P. Multiparametric Probing of Microenvironment with Solvatochromic Fluorescent Dyes. *Methods Enzymol.* **2008**, *450*, 37−58.
(16) Grabowski, Z. R.; Rotkiewicz, K.; Rettig, W. Structural Changes Accompanying Intramolecular Electron Transfer: Focus on Twisted Intramolecular Charge-Transfer States and Structures. *Chem. Rev.* **2003**, *103*, 3899−4032.
(17) Inoue, Y.; Jiang, P.; Tsukada, E.; Wada, T.; Shimizu, H.; Tai, A.; Ishikawa, M. Unique Dual Fluorescence of Sterically Congested Hexaalkyl Benzenehexacarboxylates: Mechanism and Application to Viscosity Probing. *J. Am. Chem. Soc.* **2002**, *124*, 6942−9.
(18) Haidekker, M. A.; Theodorakis, E. A. Environment-Sensitive Behavior of Fluorescent Molecular Rotors. *J. Biol. Eng.* **2010**, *4*, 11.
(19) Kasha, M. Characterization of Electronic Transitions in Complex Molecules. *Discuss. Faraday Soc.* **1950**, *9*, 14−19.
(20) Signore, G.; Nifosi, R.; Albertazzi, L.; Storti, B.; Bizzarri, R. Polarity-Sensitive Coumarins Tailored to Live Cell Imaging. *J. Am. Chem. Soc.* **2010**, *132*, 1276−88.
(21) Velapoldi, R. A.; Tonnesen, H. H. Corrected Emission Spectra and Quantum Yields for a Series of Fluorescent Compounds in the Visible Spectral Region. *J. Fluoresc.* **2004**, *14*, 465−72.
(22) Birch, D. J.; Imhof, R. E. Time-Domain Fluorescence Spectroscopy Using Time-Correlated Single-Photon Counting. In *Topics in Fluorescence Spectroscopy*, Lakowicz, J. R., Ed.; Kluwer Academic Publisher: New York, 1999; pp 1−96.
(23) Beechem, J. M.; Ameloot, M.; Brand, L. Global and Target Analysis of Complex Decay Phenomena. *Anal. Instrum.* **1985**, *14*, 379−402.
(24) Polli, D.; Antognazza, M. R.; Brida, D.; Lanzani, G.; Cerullo, G.; De Silvestri, S. Broadband Pump-Probe Spectroscopy with Sub-10-Fs Resolution for Probing Ultrafast Internal Conversion and Coherent Phonons in Carotenoids. *Chem. Phys.* **2008**, *350*, 45−55.
(25) Runge, E.; Gross, E. K. U. Density-Functional Theory for Time-Dependent Systems. *Phys. Rev. Lett.* **1984**, *52*, 997−1000.
(26) Casida, M. E. Time-Dependent Density-Functional Response Theory for Molecules. In *Recent Advances in Density Functional Methods Part 1*; Chong, D. P., Ed.; Recent Advancdes in Computational Chemistry 1; World Scientific, Singapore, 1995; pp 155192
(27) Adamo, C.; Barone, V. Toward Reliable Density Functional Methods without Adjustable Parameters: The Pbe0Model. *J. Chem. Phys.* **1999**, *110*, 6158−6170.
(28) Ernzerhof, M.; Scuseria, G. E. Assessment of the Perdew−Burke−Ernzerhof Exchange-Correlation Functional. *J. Chem. Phys.* **1999**, *110*, 5029−5036.
(29) Becke, A. D. Density-Functional Thermochemistry. Iii. The Role of Exact Exchange. *J. Chem. Phys.* **1993**, *98*, 5648−5652.
(30) Stephens, P. J.; Devlin, F. J.; Chabalowski, C. F.; Frisch, M. J. Ab-Initio Calculation of Vibrational Absorption and Circular-Dichroism Spectra Using Density-Functional Force-Fields. *J. Phys. Chem.* **1994**, *98*, 11623−11627.
(31) Yanai, T.; Tew, D. P.; Handy, N. C. A New Hybrid Exchange−Correlation Functional Using the Coulomb-Attenuating Method (Cam-B3lyp). *Chem. Phys. Lett.* **2004**, *393*, 51−57.
(32) Barone, V.; Cossi, M. Quantum Calculation of Molecular Energies and Energy Gradients in Solution by a Conductor Solvent Model. *J. Phys. Chem. A* **1998**, *102*, 1995−2001.
(33) Cossi, M.; Rega, N.; Scalmani, G.; Barone, V. Energies, Structures, and Electronic Properties of Molecules in Solution with the C-Pcm Solvation Model. *J. Comput. Chem.* **2003**, *24*, 669−681.
(34) Klamt, A.; Schuurmann, G. Cosmo: A New Approach to Dielectric Screening in Solvents with Explicit Expressions for the Screening Energy and Its Gradient. *J. Chem. Soc., Perkin Trans. 2* **1993**, 799−799.
(35) Improta, R.; Barone, V.; Scalmani, G.; Frisch, M. J.; State-Specific, A. Polarizable Continuum Model Time Dependent Density Functional Theory Method for Excited State Calculations in Solution. *J. Chem. Phys.* **2006**, *125*, 054103−1−9.
(36) Improta, R.; Scalmani, G.; Frisch, M. J.; Barone, V. Toward Effective and Reliable Fluorescence Energies in Solution by a New

State Specific Polarizable Continuum Model Time Dependent Density Functional Theory Approach. *J. Chem. Phys.* **2007**, 074504−1−9.
(37) Bloino, J.; Biczysko, M.; Santoro, F.; Barone, V. General Approach to Compute Vibrationally Resolved One-Photon Electronic Spectra. *J. Chem. Theory Comput.* **2010**, *6*, 1256−1274.
(38) Barone, V.; Baiardi, A.; Biczysko, M.; Bloino, J.; Cappelli, C.; Lipparini, F. Implementation and Validation of a Multi-Purpose Virtual Spectrometer for Large Systems in Complex Environments. *Phys. Chem. Chem. Phys.* **2012**, *14*, 12404−12422.
(39) Frisch, M. J., et al., *Gaussian 09*, Revision B.01; Gaussian Inc.: Wallingford CT, 2009.
(40) Sengwa, R. J.; Kaur, K.; Chaudhary, R. Dielectric Properties of Low Molecular Weight Poly(Ethylene Glycol)S. *Polym. Int.* **2000**, *49*, 599−608.
(41) Han, F.; Zhang, J. B.; Chen, G. H.; Wei, X. H. Density, Viscosity, and Excess Properties for Aqueous Poly(Ethylene Glycol) Solutions from (298.15 to 323.15) K. *J. Chem. Eng. Data* **2008**, *53*, 2598−2601.
(42) Lofroth, J. E. Time-Resolved Emission-Spectra, Decay-Associated Spectra, and Species-Associated Spectra. *J. Phys. Chem.* **1986**, *90*, 1160−1168.
(43) Schuddeboom, W.; Jonker, S. A.; Warman, J. M.; Leinhos, U.; Kuhnle, W.; Zachariasse, K. A. Excited-State Dipole-Moments of Dual Fluorescent 4-(Dialkylamino)Benzonitriles - Influence of Alkyl Chain-Length and Effective Solvent Polarity. *J. Phys. Chem.* **1992**, *96*, 10809−10819.
(44) Horng, M. L.; Gardecki, J. A.; Papazyan, A.; Maroncelli, M. Subpicosecond Measurements of Polar Solvation Dynamics - Coumarin-153 Revisited. *J. Phys. Chem.* **1995**, *99*, 17311−17337.
(45) Horng, M. L.; Gardecki, J. A.; Maroncelli, M. Rotational Dynamics of Coumarin 153: Time-Dependent Friction, Dielectric Friction, and Other Nonhydrodynamic Effects. *J. Phys. Chem. A* **1997**, *101*, 1030−1047.
(46) Gaus, K.; Zech, T.; Harder, T. Visualizing Membrane Microdomains by Laurdan 2-Photon Microscopy. *Mol. Membr. Biol.* **2006**, *23*, 41−8.
(47) Signore, G.; Abbandonato, G.; Storti, B.; Stockl, M.; Subramaniam, V.; Bizzarri, R. Imaging the Static Dielectric Constant in Vitro and in Living Cells by a Bioconjugable Gfp Chromophore Analog. *Chem. Commun.* **2013**, *49*, 1723−5.
(48) Signore, G.; Nifosi, R.; Albertazzi, L.; Bizzarri, R. A Novel Coumarin Fluorescent Sensor to Probe Polarity around Biomolecules. *J. Biomed. Nanotechnol.* **2009**, *5*, 722−9.